Supporting Information for

Self-organized sulfide-driven traveling pulses shape seagrass meadows

D. Ruiz-Reynés, E. Mayol, T. Sintes, I.E. Hendriks, E. Hernández-García, C.M. Duarte, N. Marbà, and D. Gomila

Damià Gomila.
E-mail: damia@ifisc.uib-csic.es

This PDF file includes:

Supporting text
Figs. S1 to S5
Legends for Movies S1 to S4
SI References

Other supporting materials for this manuscript include the following:

Movies S1 to S4

Supporting Information Text

Study site. The experimental study was conducted at Pollença bay (Mallorca Island, Western Mediterranean), a sheltered bay exposed to high human pressure (1) with the sea bottom colonized by *Posidonia oceanica*. At the northeast of the bay and at 2-3 m water depth, *P. oceanica* grows forming rings which are delimited by bare sand or *P. oceanica* dead matte colonized by sparse vegetation of the macroalgae *Caulerpa prolifera* and the seagrass *Cymodocea nodosa*. The measurements for this study were conducted on six *P. oceanica* rings located at 150-250 meters from the coast, although there is a wave breaker in between (around 75 and 150 meters of distance to the rings), in September 2021.

Fieldwork sampling. In each selected *P. oceanica* ring, we laid one transect perpendicular to the vegetation front from one meter before the inner edge of the front to one meter after the outer edge of it. Along each transect, and every 20 cm, we measured *P. oceanica* shoot density in 25 × 25 cm squares and collected a sample of the top 10 cm of sediment with 2.6 cm diameter cores. The sediment was fixed in 1 M zinc acetate (vol:vol). The samples were stored frozen until distillation. Acid volatile sulfide (AVS) was liberated by the addition of 6 M HCl (in 50% ethanol) and was trapped in zinc acetate, following Fossing & Jørgensen (1989) (2) and Marbà et al. (2007) (3). The concentrations of AVS pools from the traps were determined spectrophotometrically according to Cline (1969) (4).

The sulfides in the AVS pool can contain sulfides bound to Fe as FeS. However, the carbonate sediment in the coasts of Mallorca, and in the Pollença bay in particular, are strongly iron-depleted, so the fraction of sulfides bound to Fe as FeS should be very small in this case (13, 19). Therefore we consider the concentration of AVS pools to be a fair approximation of the porewater sulfide concentration at this location, which corresponds to the sulfide connectration described by the model.

At the inner and outer edges of each ring, we collected three shoots for determination of δ^{34}S in the leaves. In the laboratory, we scraped the epiphytes from the leaves, soaked the leaves into miliQ water for 5 minutes to remove the salts, and oven-dried them at 60°C for 48h. The δ^{34}S in the samples was determined at the Iso Analytical Limited Lab (UK) using a continuous flow isotope ratio mass spectrometer interfaced with an elemental analyzer (EA-IRMS).

Model for coupled vegetation density and sulfide concentration dynamics

We build on a previous model (5) for the dynamics of the vegetation density $n \equiv n(x, y, t)$ to include the effects of hydrogen sulfide concentration $S \equiv S(x, y, t)$.

The time evolution of the vegetation is described by the following partial differential equation:

$$\partial_t n = (\omega_b - \omega_d(n, S))n + d_0\nabla^2 n + d_1 n\nabla^2 n + d_1|\nabla n|^2, \quad [1]$$

where ω_b refers to the branching rate, the terms with spatial derivatives encode clonal growth mechanisms (5), with $\nabla = (\partial_x, \partial_y)$, and the mortality rate ω_d depends not only on the local density but also on the porewater hydrogen sulfide concentration S in μM. Direct measurements of demographic rates of *P. oceanica* exposed to different sulfide concentrations indicate a clear effect of sulfides on mortality, reducing the shoot population growth rate up to 15% when exposed to moderate sulfide concentrations around $30\mu M$ (6). We include this effect in our model increasing the mortality ω_d proportionally to the sulfide concentration S:

$$\omega_d(n, S) = \omega_{d0} - \frac{\omega_{d0} an}{1 + an} + bn^2 + \gamma S. \quad [2]$$

Parameter γ is the sensitivity of the plant to sulfide concentration and measures the increment of the mortality rate for each unit of sulfide concentration. ω_{d0} represents the intrinsic mortality rate of a shoot in the absence of neighboring plants, determining the typical lifespan of a single shoot, which can depend on external factors such as temperature, salinity, or light availability (7, 8). Moreover, local density-dependent effects decreasing mortality (facilitation) appear as a result of stress amelioration, for example reducing wave energy within the meadow or contributing to stabilize or trap sediments (9). Facilitation is included via the term $\frac{\mu an}{1+an}$ which grows linearly with n for low densities and saturates to the value of μ which corresponds to the maximum facilitation. To avoid unrealistic growth, facilitation can not overcome mortality, since it would represent the creation of plants. Hence, $\mu \leq \omega_{d0}$ which for simplicity we choose $\mu = \omega_{d0}$. The third term in the right hand side of (2) represents negative effects increasing mortality with density, as a result from self-shading or competition due to resource depletion, determining the maximum density in the meadow.

The evolution of the sulfide concentration is dominated by three processes, the diffusion of organic matter produced by the plant, production of sulfides due to decomposition, and sulfide removal. In fact, it is possible to describe the evolution of both organic matter and sulfides with two equations, similarly to what is done in other models (10), where organic matter diffuses to the surroundings and generates sulfides, which also are able to diffuse on a slower time scale through the sediment. However, we prefer to use a simpler description accounting only for sulfide concentration, thus, effectively, sulfides are produced exogenously at a constant rate and proportionally to death plants, and its diffusion encompasses not only diffusion of sulfides in the sediment but diffusion of organic matter in the water column due to the flow. The evolution of the concentration of sulfide $S \equiv S(\vec{x}, t)$ is then described by

$$\partial_t S = c_s\omega_d(n, S)n + P_s - \delta_s S - \delta_o nS + D_s\nabla^2 S, \quad [3]$$

where c_s accounts for the increment of sulfide concentration for each dead shoot, $\delta_s + \delta_o n$ is the rate of removal of sulfides, and D_s is the effective diffusion of sulfides. We consider all parameters to take only positive values. Thus, Eqs. (1-3) reproduce the

coupled dynamics of vegetation and sulfide concentration and determine the effect of this toxic compound on the growth of the plant.

Concerning the generation of sulfides, both exogenous carbon inputs and endogenous carbon generated by dead plants, after being buried in the first centimeters of sediment, drive sulphate reduction, resulting in increasing porewater sulfide concentrations. The sulfate reduction rate (SRR) quantifies the production of sulfide. This flux can not be directly associated to the net sulfide production, because sulfide is oxidized back again to sulfate if oxygen is present in the upper layer of the sediment. Furthermore, seagrass roots release oxygen into the sediment, particularly during day time, when the plant photosynthesizes, as a protection mechanism against sulfide intrusion (11), which increases sulfide oxidation. Hence, to determine the net production of sulfide it is necessary to consider the balance between these two processes. Seagrass sediment SRR, and sulfide and sulfate concentrations in the literature (6, 12–16) range between $100-500\ \mu M/d$, $1-300\ \mu M$, and $\sim 30\ mM$ respectively. However, there are fewer estimations of the sulfide oxidation rates (12). We assume, then, the hydrogen sulfide in the sediment to be produced proportionally to the density of dead plants, $c_s\omega_d(n,S)n$, and introduced also exogenously at a constant rate P_s.

We distinguish two processes regarding sulfide removal. First, sulfide is removed through combination with iron to form pyrite (FeS_2), which is dependent on iron concentration and independent of shoot density. Second, density-dependent processes include direct absorption through the roots, resulting in intoxication of the plant (17), and sulfide oxidation to sulfate due to oxygen released by the plant into the sediment, both of which are assumed to be proportional to shoot density and sulfide concentration. The contribution of each process to the total removal is unclear and highly dependent on the properties of the substrate. In particular, carbonate sediments, characterized by low iron availability and slow sulfide removal, are associated with high seagrass vulnerability to sulfide intrusion (3, 6, 13, 18–20). So, porewater sulfide is removed in Eq. (3) at a constant rate δ_s, accounting for the combination with iron, and proportionally to the shoot density and sulfide concentration, $\delta_o nS$, accounting for direct absorption and sulfide oxidation.

The spatial reach of sulfide impacts on seagrass have been quantified in fish farms, providing insights into the spatial scale of sulfide effects on *P. oceanica* (21–24). The production of biomass at a given position can affect the growth at important distances due to either the direct diffusion of sulfides in the substrate or within plants, or the transport of decomposing organic matter by the water. Nevertheless, the real spatial range of sulfide effects is uncertain yet, ranging from tens of centimeters to tens of meters. Due to the limited evidence, we describe this process as regular diffusion, exploring the effects of different diffusion constant values D_s on the spatiotemporal dynamics.

Parametrization for *Posidona oceanica*. The values of the parameters characterizing the clonal growth of several seagrasses, namely the branching rate and angle, and the elongation velocity of the rhizome are available in the literature. For *P. oceanica* we take the branching rate $\omega_b = 0.6$ year^{-1}, the branching angle $\phi_b = 49^\circ$ ($\sim 45^\circ$ for simplicity) and the elongation velocity of the rhizome $\nu = 6.11$ cm/year (25). In order to show that rings can form it is useful to explore the parameter ω_b in the range $\sim 0.06-0.6$, which can be justified by measurements indicating a ten fold increment close to the coast. The coefficients of the terms with spatial derivatives can be approximately determined from these parameters (5). Here we take $d_0 = 31.1$ cm^2 year^{-1}, and $d_1 = 1.04\times 10^2$ cm^4 year^{-1}. The taken value of d_0 leads, for $\omega_d \sim \omega_b$, to a vegetation diffusion length of 7 cm, compatible with the growth of a rizhome over a year for *Posidonia oceanica*.

The parameter $b = 6.67$ cm^4 year^{-1} is chosen to have the maximum density of 3000 shoots/m^2 with no sources of mortality other than density dependent terms ($\omega_{d0} = \gamma = 0$). Equivalently, to determine the scale for the shoot density we set $\sqrt{\omega_b/b} = 0.3$ shoots/cm^2. The range of bistability is mainly controlled by parameter a. Given the limited evidence, we choose this parameter such that the change in mortality ω_{d0} within the bistable range is comparable to the branching rate $\sim \omega_b$ for the other parameters fixed, similarly to what was done in a previous work (26).

Estimates of sulfide removal $\delta_s + \delta_o n \sim 1$ year^{-1} were determined using time series (3). The variability in estimating such parameters is very large and some estimates are bigger than the values of the parameters δ_s and δ_o compatible with the existence of excitable pulses. According to Eq. (8), the parameter δ_s, which is the most relevant for having excitability, must be smaller than ω_b, what means that the evolution of sulfides is slower than the time scale of vegetation. Given the limited precision of the data avaliable in the literature, we take $\delta_s = 3.6\times 10^{-2}$ year^{-1} and $\delta_o = 6\times 10^{-2}$ year^{-1} cm^2 to set the system in the excitable region. This value is smaller than a previous estimation (3) but reasonable within the variability of sulfide concentration measures. The production of sulfides P_s is included in the model to allow to reproduce a constant background of sulfides. In our measurement this background concentration, determined using the values of sulfide concentration outside of the ring, is $S_0 = P_s/\delta_s \sim 31.4\ \mu$M, and we set $P_s = 1.13\ \mu$M year^{-1}. Parameter $c_s \sim 30.6\mu$M cm^2 is set to fit the scale of the measured sediment sulfide concentrations, ensuring the order of magnitude, while being in agreement with other previous experimental measurements (6). To determine the values of c_s we have used the relation between the sulfide concentration and vegetation density for the stationary homogeneous solution $S^* = \frac{c_s\omega_b n^* + P_s}{\delta_s + \delta_o n^*}$, which linearized allows to estimate an order of magnitude for c_s from the relation between sulfide concentration and density determined experimentally $S_{exp} \sim P_s/\delta_s + (c_s\omega_b\delta_s - P_s\delta_o)/\delta_s^2 n_{exp}$ with the other parameters fixed. Regarding sulfide diffusion, there are no precise estimates of the diffusion coefficient of sulfides, which we have changed significantly to investigate its role in the dynamics. The precise values used are given in the figure captions. The value used in Fig. 3 to generate traveling pulses is $D_s = 3.6$ cm^2 year^{-1} which correspond to a diffusion length $\sqrt{D_s/\delta_s} = 0.1$ m, compatible with diffusion through the sediment.

Finally, the sensitivity to sulfides is one of our main control parameters and we vary it significantly to explore the different dynamical regimes. The precise values are indicated in the figures. The value used in the numerical simulations of the rings $\gamma = 7.19\times 10^{-3}\ \mu$ M^{-1} year^{-1} ($\gamma\frac{c_s}{\sqrt{\omega_b b}} = 1.1\times 10^{-1}$), is less than twice (1.8 fold) the experimental value of $\gamma = 4.1\times 10^{-3}$

μ M^{-1} year^{-1} ($\gamma\frac{c_s}{\sqrt{\omega_b b}} = 6.27\times10^{-2}$) estimated in the literature (6). Moreover, it is worth mentioning the experimental value would also exhibit excitability although in a smaller range of mortality. We also point out that the relevant parameter to observe a given dynamical regime is not γ alone, but the product γc_s (see Fig. 2), and c_s determines the scale of the sediment sulfide concentration. We have chosen c_s to fit the measured concentrations, but sediment sulfide concentration is highly variable over time compared to the changes in vegetation density. Therefore the values of γ used are referred to the concentrations measured in September 2021, which may not account for previous sulfide exposure. Should the concentration be higher in other periods, the effective values of γ could be lower.

Dimensionless parameters. For simplicity it is convenient to work with dimensionless units, such that time, space and density of shoots in the new units are given by: $t' = \omega_b t$, $\vec{r'} = \sqrt{\frac{\omega_b}{d_0}}\vec{r}$, $n' = \sqrt{\frac{b}{\omega_b}}n$ and $S' = \frac{1}{c_s}\sqrt{\frac{b}{\omega_b}}S$. We note that the branching rate fixes the temporal scale, the spatial scale is determined by the vegetation diffusion, the scale of the density of shoots is determined by the saturation parameter b, and, finally, the scale of sulfide concentration is determined by c_s. In the following we drop the primes from the variables and parameters expressed in the new units.

Dynamical regimes and linear stability analysis. The model given by Eqs. (1-3) describes the coupled dynamics of seagrass shoot density and porewater sulfide concentration, allowing to study the effects of instabilities on the spatial distribution of vegetation and the emerging spatiotemporal regimes. The homogeneous steady states n^* of Eqs. (1-3) are given by the solutions of the nonlinear equation $(\omega_b - \omega_d(n^*, S^*))n^* = 0$, where $S^* = \frac{c_s\omega_b n^* + P_s}{\delta_s + \delta_o n^*}$. The solutions can be multiple depending on the parameters.

Under favorable conditions (i.e. when the density-independent mortality is smaller than the branching rate $\omega_{d0}/\omega_b < 1$, light blue shaded region in Fig. 2), bare soil ($n^* = 0$), which is always a solution of the equations independently of the parameters, is unstable and vegetation grows and forms a homogeneous meadow with density $n^* = n_p^*$. Given a fixed branching rate, increasing mortality ω_{d0} leads to a reduction in the stationary value of shoot density, until large values of ω_{d0} lead to bare soil as the only possible stable configuration (white region). As a result of facilitative effects, the systems exhibits bistability at values of ω_{d0} above, but close to, the critical value ($\omega_{d0}/\omega_b = 1$) provided moderate sensitivity to sulfide concentration (γ), leading to the populated and unpopulated solutions coexisting for a range of ω_{d0} values above ω_b (dark blue shaded region in Fig. 2). In this regime an additional homogeneously populated unstable solution $n^* = n_u^*$ with an intermediate density between 0 and n_p^* exists too.

The homogeneous solutions are affected by different instabilities that determine the spatiotemporal evolution of the vegetation density. We use linear analysis to calculate the stability of the stationary homogeneous solutions by considering perturbations of the form $n = n^* + n_p$, $S = S^* + S_p$. The linearized systems reads:

$$\partial_t n_p = (\omega_b - \omega_d(n^*, S^*) + \beta(n^*))n_p - \gamma n^* S_p + (d_0 + d_1 n^*)\nabla^2 n_p, \quad [4]$$

$$\begin{aligned}\partial_t S_p = c_s(\omega_d(n^*, S^*) - \beta(n^*))n_p + (c_s\gamma n^* - \delta_s - \delta_o n^*)S_p \\ -\delta_o S^* n_p + D_s\nabla^2 S_p,\end{aligned} \quad [5]$$

where $\beta(n^*) = -2bn^* + \frac{\omega_{d0} a n^*}{(1+an^*)^2}$. Considering perturbations of the form $\sim e^{-i\vec{q}\cdot\vec{x}}$ the following eigenvalue problem results,

$$\begin{vmatrix}\omega_b - \omega_d^* + \beta^* - D_n^* q^2 - \lambda & -\gamma n^* \\ c_s(\omega_d^* - \beta^*) - \delta_o S^* & c_s\gamma n^* - \delta_s - \delta_o n^* - D_s q^2 - \lambda\end{vmatrix} = 0 \quad [6]$$

where $q^2 = \vec{q}\cdot\vec{q} = q_x^2 + q_y^2$ and $\beta^* = \beta(n^*)$, $\omega_d^* = \omega_d(n^*, S^*)$ and $D_n^* = d_0 + d_1 n^*$. Thus, the eigenvalues for the unpopulated solution ($n^* = 0$) are $\lambda = \omega_b - \omega_{d0} - \gamma Ps/\delta_s - d_0 q^2$ and $\lambda = -\delta_s - D_s q^2$. The first eigenvalue is negative for all values of q when $\omega_b > \omega_{d0} + \gamma Ps/\delta_s$, which corresponds to a transcritial bifurcation determining the stability of the unpopulated solution. The second eigenvalue, which is always negative, determines the time scale of sulfides close to the unpopulated solution being determined by the removal rate δ_s. Both eigenvalues have high-wavenumber damping given by diffusion.

The eigenvalues of the populated solutions are given by roots λ of the following characteristic polynomial:

$$\begin{aligned}\lambda^2 - \lambda(\beta^* - (D_n^* + D_s)q^2 + c_s\gamma n^* - \delta_s - \delta_o n^*) \\ -\beta^*(\delta_s + \delta_o n^*) + c_s\omega_b\gamma n^* - \gamma n^*\delta_o S^* \\ -(\beta^* D_s + D_n^*(c_s\gamma n^* - \delta_s - \delta_o n^*))q^2 \\ +D_n^* D_s q^4 = 0.\end{aligned} \quad [7]$$

Finding the roots of (7), one obtains that the homogeneous solution $n^* = n_u^*$ is always unstable, while $n^* = n_p^*$ is always stable for low enough ω_{d0}. Instead for values of ω_{d0} comparable to ω_b, and large enough sensitivity to sulfide γ, the total mortality ω_d increases significantly with increasing sulfide concentration, destabilizing the homogeneous vegetation distribution in two different ways.

On one hand, it can experience an oscillatory instability of the homogeneous meadow, a Hopf bifurcation, where vegetation experiences a periodic cycle (pink region in Fig. 2). The Hopf bifurcation can be identified by imposing $\lambda(q = 0) = i\omega$ with $\omega \in \mathbb{R}$ in Eq. (7) and determining this way the parameter regimes leading to oscillatory behavior. The presence of oscillations

can be easily understood considering the negative feedback loop between vegetation and sulfides. The growth of vegetation leads to sulfide production with a certain time lag, which beyond a threshold concentration causes vegetation density to decline. The production of sulfides, then, decreases as well until its concentration becomes low enough to allow the vegetation to regrow, generating a spatially homogeneous periodic oscillation of the vegetation density and sulfide concentration.

On the other hand, the homogeneous solution can also experience a Turing instability, which is calculated imposing the conditions $Re[\lambda(q)] = Re[\frac{\partial\lambda(q)}{\partial q}] = 0$ on Eq. (7) and it is indicated in Fig. 2 with dashed lines for different values of the sulfide diffusion constant D_s. As a result of this instability spatial modulations grow leading to the formation of regular patterns. The spatiotemporal dynamics resulting from these two combined instabilities leads to a very complex Turing-Hopf behavior (27). In this work we focus on the case in which the dynamics is dominated by the Hopf bifurcation, which corresponds to low values of D_s (Fig. 2), in particular, values of the interaction length of vegetation driven by sulfides $\sqrt{D_s/\delta_s}$ smaller than half meter. In this case, starting from a populated homogeneous solution and increasing ω_{d0}, the Hopf bifurcation occurs first and the oscillatory dynamics dominates over pattern formation.

In the bistable regime the homogeneous steady state n_p^* coexists with the unpopulated state $n^* = 0$ and the unstable homogeneous steady state n_u^*. The intermediate density n_u^* acts as a threshold for the facilitation to operate and sustain an homogeneous meadow. On top of this, the presence of a cycle bifurcating from the Hopf instability of the upper homogeneous solution n_p^*, and whose amplitude grows as mortality is increased, can lead to a situation in which, during the cycle, the density reaches the value of the unstable solution n_u^*. At this point the cycle is destroyed, since facilitative interactions are not strong enough to support vegetation for densities below n_u^*. This transition, known as homoclinic bifurcation, is a global bifurcation that changes the dynamics of the system drastically. Close to the onset of the homoclinic bifurcation, the dynamics of the periodic oscillation become very slow for densities close to n_u^*, increasing the period of the oscillations, which diverges at threshold (28). When the homoclinic transition is crossed and there is no limit cycle (orange region in Fig. 2), the dynamics becomes excitable. Since, n_u^* acts as a threshold for the vegetation to grow, vegetation will decrease exponentially to zero below this threshold, while densities larger than n_u^* will allow the vegetation to grow, increasing also the sulfide concentration until a certain point in which mortality overshoots leading to vegetation density to decrease again below n_u^*, and then to zero. This excitable excursion reproduces a single cycle of the former oscillatory state. In this excitable regime the final state is always bare soil independently of the initial density, but if the initial vegetation is dense enough to overcome the threshold, then the system produces a pulse of vegetation before ending up in bare soil.

The curve delimiting the homoclinic bifurcation in parameter space (orange region in Fig. 2) is born at two Takens-Bogdanov ($TB_{1,2}$) points, where the Hopf coincides with the saddle node bifurcation. Writing the stationary condition as $\omega_{d0} \equiv \omega_{d0}(n^*)$ one can impose the saddle node condition $\frac{\partial\omega_{d0}(n^*)}{\partial n^*} = 0$ and introduce it in Eq. (7). This forces one of the eigenvalues to be zero. Imposing the second eigenvalue to be zero allows to determines the TB points. The three condition give involved relations which are solved numerically.

Under the right conditions, an analytical criteria for the existence of a TB can be derived. In general the maximum vegetation density is determined by the term bn^2 present in the total mortality. However the term γS also prevents an unlimited growth determining the maximum value of the density. Under these circumstances a good approximation is to neglect the term bn^2. For $\delta_o = P_s = 0$, this allows to find an approximated value of the mortality at which the TB_1 takes place:

$$\frac{\omega_{d0,\mathrm{TB}_1}}{\omega_b} \approx \frac{1}{1-\frac{\delta_s^2}{\omega_b^2}} \qquad [8]$$

Since the TB_1 point is the origin of the homoclinic bifurcation, the existence of a TB point is good indication of the existence of excitable dynamics in a nearby parameter region. This requires the right hand side of Eq. (8) to be positive, as the mortality and branching rates take positive values only. Thus, excitability is more easily observed for $\delta_s < \omega_b$. This implies that the formation of rings are most likely to occur if the removal rate of sulfides δ_s is smaller than the branching rate of the plant ω_b.

Numerical simulations. The model described by (1), (2) and (3) is a system of two coupled partial differential equations (PDEs) which is integrated in time with a pseudo-spectral method (29). We consider a squared grid with N_x and N_y grid points with periodic boundary conditions and we integrate the linear terms in Fourier space exactly, while the nonlinear terms are integrated using a second-order in time approximation.

The excitable region is calculated using numerical simulations for the temporal systems where the diffusion in space has not been considered. Starting from the stationary populated solution n^*, S^* plus a small perturbation as initial condition we led the system time evolve for long times and compute the amplitude of the limit cycle. Following this procedure for different values of ω_{d0} in the bistable range one can identify when the minimum density of the limit cycle coincides with the value of the unstable branch n_u^*. This process is repeated for different values of the parameter γ to identify the homoclinic bifurcation in the phase diagram in Fig. 2.

Numerical simulations of excitable pulses or rings are performed using a grid of size $N_x = N_y = 512$ starting with an initial condition with $S(\vec{x}) = S_0$ and with spots of vegetation located at different positions where the density n follows a Gaussian function in two dimensions where the maximum density has a value of the density equal or greater than n_u^* for each parameter set. Neither the width of the Gaussian nor the initial position have effect on the final ring. A different initial spatial distribution has been used capturing the details of vegetation from ortophotos. The images have been processed in gray scale filtering regions with vegetation over a certain threshold and converted to a binary array $N_x = N_y = 1024$ with value equal to one for the position of vegetation. A diffusive filter has been applied to obtain soft transitions at the interfaces by multiplying by

$e^{-k^2 t}$ the Fourier amplitudes A_k of the array, where k is the wavenumber and t controls the softness of the interfaces. Finally, multiplying the values of the array by the stationary value of the density n^* for each parameter set, the array has been scaled to obtain the desired values of the maximum of the vegetation density for the initial condition.

Fig. S1. Aerial image of the study site. Drone image of the study site in Pollença bay showing the environment where the vegetation patterns of $Posidonia\ oceanica$ develop.

Fig. S2. General aerial view of the patterns observed in the $Posidonia\ oceanica$ meadows present in the Pollença bay.

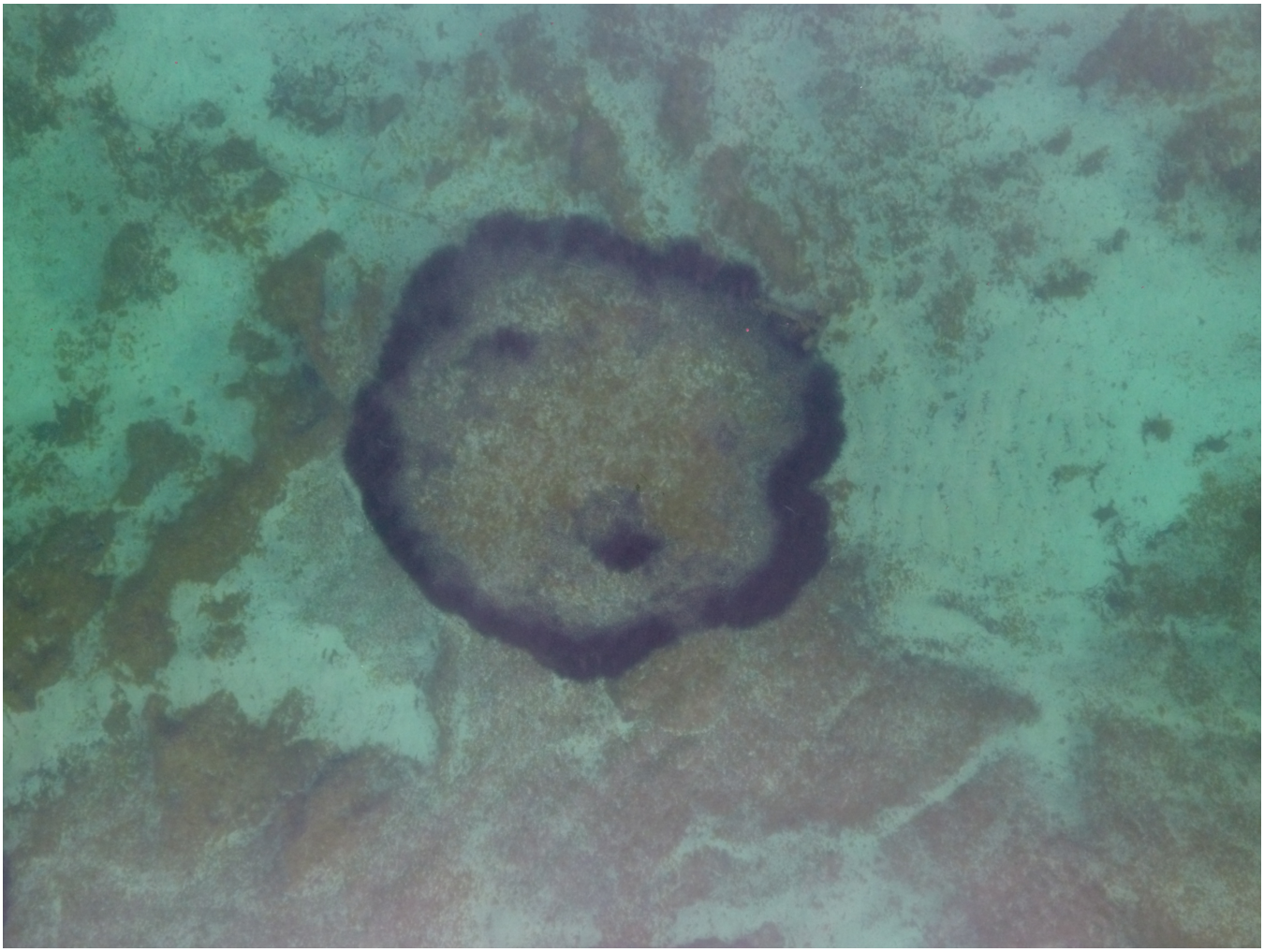

Fig. S3. Excitable ring. High-resolution 2021 drone image of an excitable ring of $Posidonia\ oceanica$ in the Pollença bay.

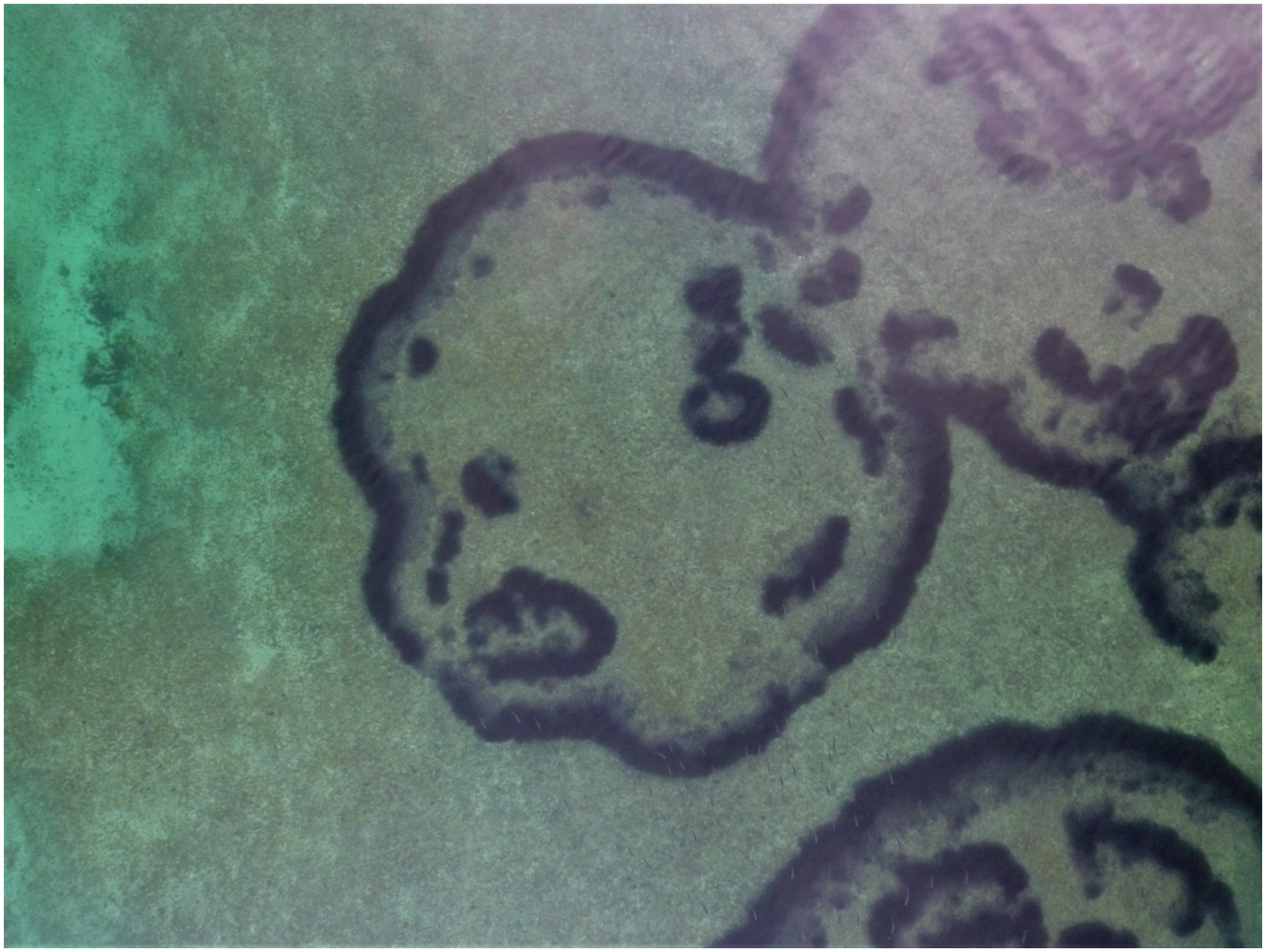

Fig. S4. Collision of two rings. High-resolution 2021 drone image of the region where two excitable rings collided.

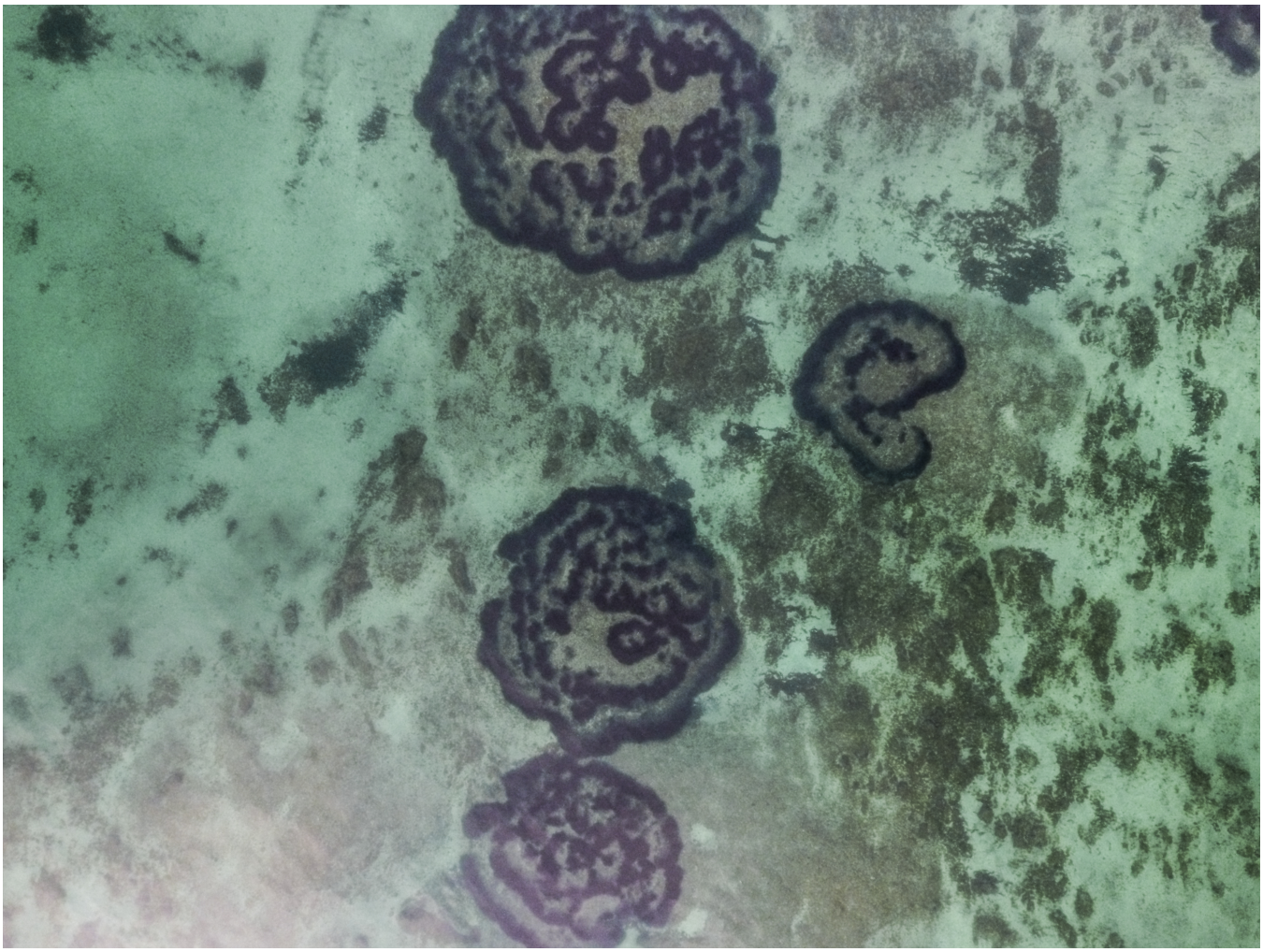

Fig. S5. Spiral of $Posidonia\ oceanica$. High-resolution 2021 drone image showing a spiral of $Posidonia\ oceanica$ and other disordered patterns as a result of the excitable dynamics.

Movie S1. Time evolution of excitable rings under spatially homogeneous mortality: Movie of the simulation shown in Figs. 3 (a-e) for homogeneous mortality conditions starting from initial conditions resembling aerial pictures of the vegetation from 1973. A collision of two rings is observed during the evolution.

Movie S2. Time evolution of excitable rings under spatially heterogeneous mortality conditions: Movie of the simulations shown in Figs. 3 (f-j) for spatially heterogeneous mortality conditions starting from vegetation initial conditions resembling aerial pictures from 1973.

Movie S3. Animation of aerial images of the study site in Pollença bay from 1973 to 2018 showing the actual evolution of the spatial distribution of vegetation patterns.

Movie S4. Animation showing a zoom of the collision of two excitable rings from historic aerial images from 1973 to 2018.

References

1. I Mazarrasa, N Marbà, J Garcia-Orellana, P Masqué, CM Arias-Ortiz, Ariane nad Duarte, Dynamics of carbon sources supporting burial in seagrass sediments under increasing anthropogenic pressure. *Limnol. Oceanogr.* **62**, 1451–1465 (2017).
2. H Fossing, BB Jørgensen, Measurement of bacterial sulfate reduction in sediments: evaluation of a single-step chromium reduction method. *Biogeochemistry* **8**, 205–222 (1989).
3. N Marbà, et al., Iron additions reduce sulfide intrusion and reverse seagrass (*Posidonia oceanica*) decline in carbonate sediments. *Ecosystems* **10**, 745–756 (2007).
4. JD Cline, Spectrophotometric determination of hydrogen sulfide in natural waters 1. *Limnol. Oceanogr.* **14**, 454–458 (1969).
5. D Ruiz-Reynés, F Schönsberg, E Hernández-García, D Gomila, General model for vegetation patterns including rhizome growth. *Phys. Rev. Res.* **2**, 023402 (2020).
6. ML Calleja, N Marbà, CM Duarte, The relationship between seagrass (*Posidonia oceanica*) decline and sulfide porewater concentration in carbonate sediments. *Estuarine, Coast. Shelf Sci.* **73**, 583–588 (2007).
7. N Marbà, CM Duarte, Mediterranean warming triggers seagrass (*Posidonia oceanica*) shoot mortality. *Glob. Chang. Biol.* **16**, 2366–2375 (2010).
8. CM Duarte, J Kalff, Latitudinal influences on the depths of maximum colonization and maximum biomass of submerged angiosperms in lakes. *Can. J. Fish. Aquatic Sci.* **44**, 1759–1764 (1987).
9. JL Gutiérrez, et al., *Physical ecosystem engineers and the functioning of estuaries and coasts.* (Elsevier Inc.) Vol. 7, pp. 53–81 (2011).
10. J de Fouw, et al., A facultative mutualistic feedback enhances the stability of tropical intertidal seagrass beds. *Sci. Reports* **8**, 12988 (2018).
11. O Pedersen, J Borum, C Duarte, M Fortes, Oxygen dynamics in the rhizosphere of *Cymodocea rotundata*. *Mar. Ecol. Prog. Ser.* **169**, 283–288 (1998).
12. BB Jørgensen, The sulfur cycle of a coastal marine sediment (Limfjorden, Denmark). *Limnol. Oceanogr.* **22**, 814–832 (1977).
13. M Holmer, CM Duarte, N Marbà, Sulfur cycling and seagrass (*Posidonia oceanica*) status in carbonate sediments. *Biogeochemistry* **66**, 223–239 (2003).
14. MS Frederiksen, M Holmer, J Borum, H Kennedy, Temporal and spatial variation of sulfide invasion in eelgrass (*Zostera marina*) as reflected by its sulfur isotopic composition. *Limnol. Oceanogr.* **51**, 2308–2318 (2006).
15. BB Jørgensen, Mineralization of organic matter in the sea bed—the role of sulphate reduction. *Nature* **296**, 643–645 (1982).
16. J Borum, et al., Eelgrass fairy rings: sulfide as inhibiting agent. *Mar. Biol.* **161**, 351–358 (2014).
17. O Pedersen, T Binzer, J Borum, Sulphide intrusion in eelgrass (*Zostera marina* L.). *Plant, Cell Environ.* **27**, 595–602 (2004).
18. M Holmer, P Storkholm, Sulphate reduction and sulphur cycling in lake sediments: a review. *Freshw. Biol.* **46**, 431–451 (2001).
19. M Holmer, CM Duarte, N Marbà, Iron additions reduce sulfate reduction rates and improve seagrass growth on organic-enriched carbonate sediments. *Ecosystems* **8**, 721–730 (2005).
20. N Marbà, et al., Sedimentary iron inputs stimulate seagrass (*Posidonia oceanica*) population growth in carbonate sediments. *Estuarine, Coast. Shelf Sci.* **76**, 710–713 (2008).
21. MS Frederiksen, M Holmer, E Díaz-Almela, N Marbà, CM Duarte, Sulfide invasion in the seagrass *Posidonia oceanica* at Mediterranean fish farms: assessment using stable sulfur isotopes. *Mar. Ecol. Prog. Ser.* **345**, 93–104 (2007).
22. M Holmer, MS Frederiksen, Stimulation of sulfate reduction rates in Mediterranean fish farm sediments inhabited by the seagrass *Posidonia oceanica*. *Biogeochemistry* **85**, 169–184 (2007).
23. M Holmer, et al., Sedimentation of organic matter from fish farms in oligotrophic Mediterranean assessed through bulk and stable isotope (δ13C and δ15N) analyses. *Aquaculture* **262**, 268–280 (2007).

24. M Holmer, et al., Effects of fish farm waste on *Posidonia oceanica* meadows: synthesis and provision of monitoring and management tools. *Mar. Pollut. Bull.* **56**, 1618–1629 (2008).
25. T Sintes, N Marbà, CM Duarte, Modeling nonlinear seagrass clonal growth: Assessing the efficiency of space occupation across the seagrass flora. *Estuaries Coasts* **29**, 72–80 (2006).
26. D Ruiz-Reynés, et al., Fairy circle landscapes under the sea. *Sci. Adv.* **3**, e1603262 (2017).
27. D Walgraef, *Spatio-temporal pattern formation: with examples from physics, chemistry, and materials science.* (Springer-Verlag, New York), p. 309 (1997).
28. A Arinyo-i Prats, P Moreno-Spiegelberg, M Matías, D Gomila, Traveling pulses in Class-I excitable media. *Phys. Rev. E* **104**, L052203 (2021).
29. R Montagne, E Hernández-García, A Amengual, M San Miguel, Wound-up phase turbulence in the complex Ginzburg-Landau equation. *Phys. Rev. E* **56**, 151–167 (1997).